Acta Materialia 263 (2024) 119465

Contents lists available at ScienceDirect

Acta Materialia

journal homepage: www.elsevier.com/locate/actamat

Full length article

Silicon phase transitions in nanoindentation: Advanced molecular dynamics simulations with machine learning phase recognition

Guojia Ge [a,b,1], Fabrizio Rovaris [b,1,*], Daniele Lanzoni [b], Luca Barbisan [b], Xiaobin Tang [a], Leo Miglio [b], Anna Marzegalli [b], Emilio Scalise [b], Francesco Montalenti [b]

[a] Department of Nuclear Science & Technology, Nanjing University of Aeronautics and Astronautics, Nanjing, 211106, China
[b] Department of Materials Science, University of Milano-Bicocca, Via R. Cozzi 55, I-20125, Milano, Italy

ARTICLE INFO

Keywords:
Nanoindentation
Molecular dynamics
Machine learning
Phase transition

ABSTRACT

Closing the gap between experiments and simulations in the investigation of high-pressure silicon phase transitions calls for advanced, new-generation modeling approaches. By exploiting massive parallelization, we here provide molecular dynamics (MD) simulations of Si nanoindentation based on the Gaussian Approximation Potential (GAP). Results are analyzed by exploiting a customized Neural Network Phase Recognition (NN-PR) approach, helping to shed light on the phase transitions occurring during the simulations. Our results show that GAP provides a realistic description of silicon phase transitions. With the support of NN-PR method, the formation mechanism and stability of high-pressure phases are comprehensively studied. Additionally, we also show how simulations based on the less demanding and widely-used Tersoff potential are still useful to investigate the role played by the indenter tip modeling. However, high-pressure phases obtained with GAP are more consistent with observations made in nanoindentation experiments, removing a spurious phase that is shown by Tersoff simulations. This behavior is explained on the base of relative phase stability with comparison with Density Functional Theory (DFT) calculations. This work provides insight into the application of state-of-the-art Machine Learning (ML) methods on nanoindentation simulations, enabling further understanding of the phase transition mechanisms in silicon.

1. Introduction

Silicon is the most important material for the semiconductor industry and understanding its mechanical behavior and deformation mechanisms is critical for the optimization of the design and production of Si-based devices. While being commonly known as a brittle material at room conditions, silicon can also exhibit a ductile behavior under certain loading and temperature conditions [1,2]. This behavior results from complex plastic mechanisms that may include slip [3,4], dislocations nucleation [5] and twinning [5,6] but are mostly driven by structural Phase Transitions (PTs). Silicon indeed exhibits several metastable allotropes some of which are very promising for optoelectronic Si-based devices, e.g. the BC8/R8 [7–9], the hexagonal diamond (hd) [10] and the amorphous phase (*a*Si) [11,12].

PTs in silicon under high-pressure conditions have been extensively studied in the last decades. PTs are obtained by different experimental approaches. One is the Diamond Anvil Cell (DAC) [13,14] where a nearly hydrostatic loading is imposed to a powdered sample; another possibility is the laser-driven shock compression [15]; a last, widely-used, technique is the micro/nano indentation [4,16,17], where a sample is loaded with the help of an indenter with a specific tip geometry. This last technique is particularly suited for the investigation of the PTs by the controlled application of a load (or an imposed strain rate) on a large sample. This also opens the way to an all-silicon alternative to the heterointegration of different semiconductors, promising for the exploitation of Si allotropes monolithically integrated with the existing Si-based technology. The general picture regarding Si PTs under loading and successive unloading as obtained by a nanoindentation experiment is the following: the diamond cubic structure (dc) undergoes a first PT under compressive loading ending in a metallic phase in the β-Sn structure that is about 22% denser than dc [18,19]. During unloading silicon does not transform directly to dc phase. Instead, depending on the specific unloading conditions, different metastable phases like BC8 or R8, or *a*Si are formed [4,20]. Finally, under annealing at a high enough temperature (starting from about 200 °C) these metastable phases can transform into the hd phase [21,22].

* Corresponding author.
E-mail address: fabrizio.rovaris@unimib.it (F. Rovaris).
[1] This authors equally contributed.

https://doi.org/10.1016/j.actamat.2023.119465
Received 3 September 2023; Received in revised form 18 October 2023; Accepted 23 October 2023
Available online 24 October 2023

These PTs can be analyzed by *post mortem* analysis like X-ray Raman spectroscopy [15,21,23] or Transmission Electron Microscopy (TEM). Recent experimental improvements even allow *in situ* analysis of the PTs. These analyses typically require Raman spectroscopy, probing only a shallow region of material close to the surface of the sample [19], or complex setups involving X-ray Diffraction (XRD) facilities [22,23]. A complete understanding of the phase diagram or the PTs mechanism under pressure is thus still lacking. With this respect, modeling the PT mechanisms plays a crucial role in understanding the process.

Classical Molecular Dynamics (MD) simulations can *in principle* easily capture the phase transformation process during nanoindentation. However, there are still some difficulties that preclude a proper investigation. The first issue is the limited time/space scales achievable by MD simulations. This poses severe limits particularly to the strain rates achievable by MD simulations, which are typically 6 or 7 orders of magnitude higher than the typically experimental values [18]. A multiscale modeling framework coupling MD to mesoscale approaches like Discrete Dislocation Dynamics or Crystal Plasticity represents the only way to extend time/space limitations for nanoindentation [24,25]. These approaches however are not suited for the modeling of PT mechanisms, since they lack essential atomistic details.

A second issue for the realistic modeling of PTs in Si is the lack of accurate classical interatomic potentials. One of the most widely used interatomic potentials for silicon is the Stillinger–Weber potential that has been proven to be particularly efficient in capturing dislocation-based processes, but poor in the prediction of PTs [26]. By contrast, Tersoff-type potentials [27,28] have been demonstrated by many researchers to provide reasonably accurate PTs under high-pressure conditions [29–32], but it is still not versatile enough to accurately reflect the experimental observations. Moreover, phase stability obtained by Tersoff calculations does not completely agree with formation energies as evaluated by Density Functional Theory (DFT) calculations or estimated experimentally. The most evident consequence of this is the emergence of the BCT5 phase in Tersoff indentation simulations, as further discussed below. This phase was initially identified in nanoindentation experiments (see for example Ref. [33]), possibly supported by earlier Tersoff simulation results. However, being the Raman peak associated to this phase so close to the dc one the same authors later recognized that the attribution of this peak to the BCT5 phase is unlikely [19] and identified it as a strained dc phase and referred to it as dc-2 [34].

Numerous efforts have been done to modify the original Tersoff potential in order to overcome its limitations, like the Integrated Potential (IP) proposed by Abram et al. [35] built as a combination of the Tersoff and SW potentials and the screened version of the Tersoff potential provided by Pastewka et al. [36]. Recently, interatomic potentials based on Machine Learning (ML) techniques have been developed and demonstrated to be capable of a high degree of accuracy, in some cases approaching *ab initio* predictions [37–39]. Although these ML potentials have much higher computational costs as compared to classical interatomic potentials, it is worth probing them for the simulations of nanoindentation. Different implementation of ML potentials for silicon exists. The Gaussian Approximation Potential (GAP) [37] is the first general-purpose potential reported for silicon. It is trained on a very large database that includes several metastable phases, vacancies, surfaces, point and line defects, providing a very broad scope of applicability. More recent approaches based on Neural Networks (NN) [40] or the Atomic Cluster Expansion (ACE) [38] have been demonstrated to be computationally more efficient but still questionable in terms of breadth of applications. We detailed our analysis with an alternative ML potential (PACE [38]) in the Supplementary Material Section S3.

Finally, it is important to notice that recognizing all the relevant Si allotropes obtained by nanoindentation is not an easy task *per se*. In fact, silicon has a large number of different phase structures and it is a great challenge to identify them, especially when they are mixed together and/or highly deformed. Most of the MD studies use coordination number (CN) to simply distinguish between the six-fold coordinated β-Sn, the five-fold coordinated BCT5 and the diamond cubic. Sometimes the CN method is expanded to a second shell, but still cannot cover the characteristic features of all the phases. In such cases, the radial distribution function (RDF) and bond angle distribution function (ADF) may be applied jointly. A wide number of more complex structure identification methods relying on structural functions or fingerprints have been proposed [41–45] but, to our knowledge, none of them has been demonstrated to work for all the complex Si allotropes. Alternative approaches rely on the recent advances in the field of ML in order to develop and train a flexible NN model to assess the phases based on local atomic configuration descriptors. The capability and portability of these approaches to distinguish different phases was demonstrated in Ref. [46], but limiting the application of the method to a few crystal structures: fcc, bcc, hcp, diamond cubic, hexagonal cubic and simple cubic, without considering the whole family of Si allotropes. A similar approach has been followed in this paper, training a NN to identify all the relevant Si phases that are encountered in high-pressure PTs.

In this paper, we address the two problems mentioned above by exploiting state-of-the-art ML potentials and a properly-developed NN phase recognition method. The paper is organized as follows: Section 2 describes the computational methods exploited in this work, including the setup of the MD and DFT calculations and technical details of the NN-PR approach that we developed to identify Si phases. The latter is first tested on typical cases (Section 3.1), and then shown to be crucial for the assessment of critical parameters of the indentation in Section 3.2. Finally, in Section 3.3 we discuss the effect of the interatomic potential on the simulation results, by directly comparing the Tersoff semi-empirical potential with the GAP potential.

2. Methods

2.1. Molecular dynamics simulations

Large-scale MD simulations were performed to investigate PTs in monocrystalline silicon induced by nanoindentation. The indenter tip consists of fixed atoms interacting with the silicon substrate by means of a Morse potentials. The parametrization chosen for this potential was as in Ref. [47], representing the interaction between carbon and silicon atoms. Both the Berkovich indenter and the spherical indenter geometry were considered. The indenter hit the substrate perpendicular to the (001) surface. A detailed description of the system size, as well as the parameters chosen for each simulation, can be found in Section 3. For each system the convergence of the stress field values on the lateral and bottom boundaries was carefully checked at the maximum loading condition. The substrate was divided into fixed, thermostat, and Newtonian layers. The fixed layer was located at the bottom to ensure structural stability; the thermostat layer just above the fixed layer was maintained at a constant temperature of 300 K with a Nosé–Hoover thermostat to dissipate excess thermal energy; finally, in the Newtonian layer, the motion of the atoms is based on Newton's equation. A typical timestep of 1 fs was considered in the integration of the equations of motion.

Two separate potentials were considered for the description of the interactions between silicon atoms: the extensively-used Tersoff potential [27,28] and the recently-developed GAP [48]. The nanoindentation simulations were conducted with the LAMMPS code [49] and the atomistic configurations were visualized and analyzed using the OVITO software [50].

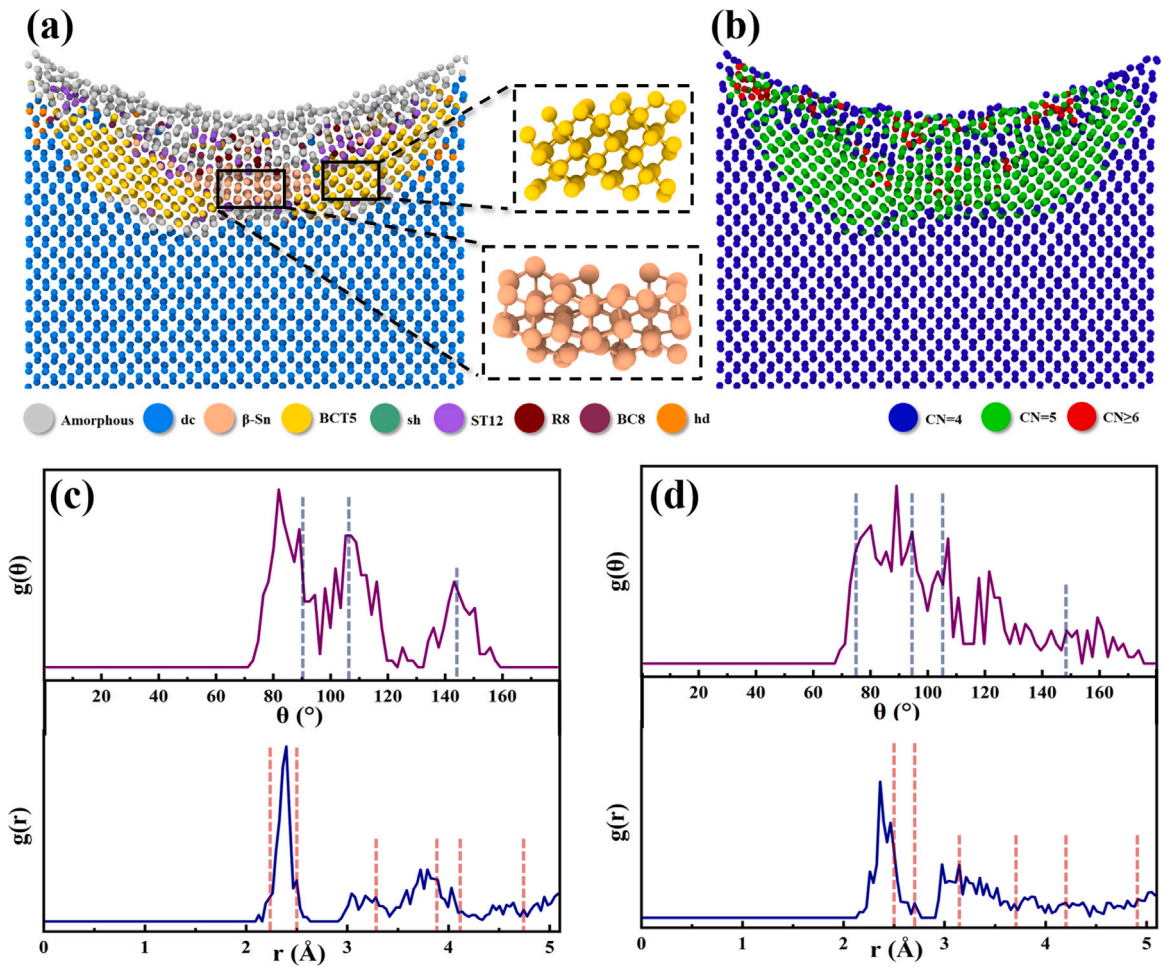

Fig. 1. Phase distribution in nanoindentation as recognized by (a) our Neural Network Phases Recognition (NN-PR) method and (b) coordination number (CN). The amorphous phase, dc, β-Sn, BCT5, sh (simple hexagonal), ST12, R8, BC8 and hd phases are distinguished by different colors, as indicated in the lower color scheme of panel (a). Coordination number coloring scheme is indicated in the lower part of panel (b); panel (c) shows the ADF and RDF of the atomic structure shown in the upper inset of panel (a), while panel (d) shows the ADF and RDF of the atomic structure in showed in the lower inset of panel (a). The dashed lines correspond to the peak of monomorphic BCT5 and β-Sn phase for panels (c) and (d), respectively. (For interpretation of the references to color in this figure legend, the reader is referred to the web version of this article.)

2.2. Density functional theory

The formation energies and structural stability of the different phases of interest in high-pressure Si phases have been calculated by means of DFT calculations based on the generalized-gradient approximation (GGA) using Perdew–Burke–Ernzerhof pseudopotentials [51] as implemented in the Vienna Computational Software Package (VASP) [52]. A plane-wave basis set with a kinetic energy cutoff of 250 eV has been used, with projector augmented wave (PAW) pseudopotentials [53], and a $32 \times 32 \times 32$ k-point mesh for sampling the Brillouin zone of the cubic diamond Si structure, and adapted according to the size of the primitive cell of the other Si phases. The convergence criterion on the total energy was set to 10^{-6} eV for the structural relaxations.

2.3. Neural network phase recognition

A feed-forward Neural Network (NN) [54] performing soft-max classification was trained and exploited for the identification of the different crystalline phases. The inputs consisted of the first 24 Smooth Overlap of Atomic Position (SOAP) components for the chemical neighborhood for each atom [55], as implemented in the DScribe python library [56]. NN output is a vector whose components can be interpreted as the confidence level for assigning each atom to a specific phase. The database was composed of approximately 10^6 examples, split in training and validation sets, representing silicon dc, hd, R8, BC8, β-Sn, sh, BCT5, ST12 and the amorphous phase. Each configuration in the database set has been obtained by adding random deformations to the equilibrium ones, obtained from the Materials Project website [57]. Validation has been performed on an independent validation set composed of 20% of the configurations randomly extracted from the database and the model was trained for 1000 epochs until the average accuracy was above 90%. The trained model has finally been implemented in OVITO for a seamless postprocessing of the simulation results. Additional details regarding the building of the database and the training of the NN-PR tool are reported in Section S1 of the Supplementary Material file of this paper. The code implementation of the phase classifier is freely available in an online repository at the following link https://bitbucket.org/frovaris/nn-pr.

3. Results and discussion

3.1. NN-PR applied to indentation simulations

In this Section, we start by showing the application of our NN-PR method to a test case of an indentation simulation. Fig. 1(a) shows the phase distribution as recognized by our NN-PR method in a simulation cell of a small Si sample indented with a spherical tip. The interatomic potential considered in this case was the Tersoff potential [27,28] while the interaction between the fixed carbon atoms of the indenter tip and

the Si substrate was described by a Morse potential [47]. Different colors represent phases as recognized by our method according to the labels in the lower part of the panel. It is evident that, except for the highly deformed region close to the surface, the NN-PR clearly distinguishes the main stable phases formed by indentation-induced PTs. Being a test case, we double-checked that the predictions were correct: we show in the two insets small regions extracted from the full structure. They can be clearly recognized as BCT5 and β-Sn structures, as correctly identified by our NN-PR method. Fig. 1(b), instead, shows the same simulated structures, but using a color-code based on their CN. The difference in information is quite evident, with the simple approach based on CN not able to fully capture the phases in the transformed regions despite the coordination number of dc, β-Sn and BCT5 being different. This is due to the high deformation reached inside the cell where the phases are distorted. Under these conditions, the CN approach is not reliable anymore. Even worst, other Si allotropes would not have been distinguishable at all based on CN, e.g. dc/hd, BC8/R8 or ST12/fcc. The advantages of our NN-PR methods are thus evident, showing better generality and robust behavior in the identification of phases.

Fig. 1(c) and (d) also show the ADF $g(\theta)$ and the RDF $g(r)$ for the BCT5 and β-Sn phase, respectively, as shown in the two insets of Fig. 1(a). The dashed vertical lines overlapped in the plots represent the peaks of the ADF and RDF for the two phases in their ground state, providing evidence that the identification of these peaks is not always straightforward in a real case scenario like a deformed configuration obtained during indentation simulations. Moreover, ADF/RDF analysis relies on a proper selection and extraction of a relevant region of the simulated domain, and many different regions should be probed in order to get a complete picture of the PTs happening during the process. This procedure is evidently not suitable as an on-the-fly algorithm that automatically detects phases during the simulations; on the contrary, NN-PR could be in principle seamlessly integrated with such automated procedures.

Based on these findings, the analysis of all simulation results presented in the following is based solely on NN-PR.

3.2. Role of the indenter

In this Section, we discuss two different aspects related to the indenter modeling. At first, we point out that some care is needed when describing the indenter–substrate interaction. Subsequently, we analyze the role of the indenter shape in causing the deformation.

The effect of interacting potential between indenter and substrate

A first set of MD simulations of indentation was performed considering a realistic Berkovich indenter tip geometry. Despite being the most common indenter in experiments it was rarely investigated in simulations [32]. We considered an initially monocrystalline silicon substrate with dimensions $49.16 \times 49.16 \times 18.38$ nm^3, made of 2 097 152 atoms. The 3D schematic diagram of the system is shown in Fig. 2(a).

In the simulation, the interaction between silicon atoms was described by the Tersoff potential. Whereas the interaction between the indenter (carbon) and substrate (silicon) was described by a Morse potential [47]. We considered two different definitions of the Morse potential: implementing the "full" expression of the Morse potential, or only the repulsive part of the potential, smoothly connecting both energy and forces to zero at the cutoff.

As shown in Fig. 2(b), the force versus indentation depth profile obtained using the original Morse potential shows an obvious negative part during the unloading process, which also can be observed in several previous MD indentation studies [29,58,59]. However, this effect is not observed in experimental data [18]. Such an issue could be due to the small size of the systems that can be investigated by MD simulations with respect to the real experimental counterparts. With the second implementation of the Morse potential, obtained by removing the attractive part between the tip and the substrate, the MD simulations closer mimic the experimental evidence. In this case, as shown in Fig. 2(b), the negative part of the force versus indentation depth curve is removed.

The effect of the tip potential definition is also clearly manifested in the PT behavior. Fig. 2(c)–(f) shows lateral cross-section views of phase distribution after maximum loading and full extraction of the tip, both using the "repulsive" (c, d) and the "original" (e, f) Morse potentials. The maximum indentation depth simulated was 5 nm, reached with an indenter tip speed of 0.2 Å/ps. The high-pressure phases, mainly β-Sn and BCT5, are formed at a very early stage. When the indentation reaches the maximum depth, Fig. 2(c) clearly shows that the β-Sn structure is concentrated at the center of the deformed region under the indenter, with the BCT5 phase surrounding it. Such a phase distribution can be easily understood by the fact that β-Sn is generated by a flattening of the tetrahedron structure of the diamond cubic silicon caused by the compressive loading along the [001] direction. Moreover, as reported by previous studies [60,61], the presence of small shear stress also promotes the transformation from dc to β-Sn. The BCT5 was formed instead by flattening the initially stepped sixfold rings of the diamond lattice onto the (110) plane [61]. With a rapid stress release during unloading, part of the BCT5 structure recovers to pristine cubic diamond, while the main part of β-Sn structure is transformed into amorphous silicon. At the end of the simulation, part of the BCT5 phase remains stable even after the indenter is fully extracted. In the simulation performed by considering the original Morse potential, the phase distribution at maximum loading is similar to the "repulsive" one, as shown in Fig. 2(e). On the contrary, the high-pressure phases are completely transformed into amorphous after fully extracting the indenter, as shown in Fig. 2(f). Because of the limited scale of the MD simulation, the negative force would "pull" the deformed atoms back to their origin site rather than releasing the stress during the unloading process. Therefore, in order to better mimic the experimental conditions on the small scales we considered only the repulsive part of the Morse potential for all the simulations described in the following.

Remarkably, by repeating several simulations based on an analogous system to that of Fig. 2, and with the help of NN-PR method, the effects of several important factors for the indentation simulations, including indent velocity and maximum depth were further explored. No significant differences in phase formation and distribution were found with the variation of indent speed in the range between 0.1 to 10 Å/ps, and maximum depth starting from 30 to 70 Å. A different behavior is observed instead for shallow penetration depths below 30 Å. In this case, the PT region obtained at the maximum loading conditions is so small that, after full extraction of the tip, almost all the phases obtained are transformed back to pristine dc or *a*Si. This behavior is shown in the Supplementary Materials Section S2 of this paper.

The effect of indenter shape

In this Section we discuss the effect of the indenter shape, considering the Berkovich and the spherical tip shapes, on the phase transitions obtained by indentation simulations. In order to easily compare the two considered tip geometries, the cross-section view along a symmetrical side of the Berkovich tip is shown in Fig. 3. The maximum depth reached is 70 Å with a speed of 0.2 Å/ps. In order to avoid the accumulation of stress at the bottom of the simulation box, the thickness of the substrate was doubled with respect to the simulation reported in Fig. 2.

When the indentation reaches the maximum depth, as shown in Fig. 3(a) and (d) for the Berkovich and spherical indenter, respectively, the β-Sn phase is formed surrounded by the BCT5 phase in both the simulations. Interestingly, the main shape-related differences appeared in the unloading process. The β-Sn structure under the Berkovich indenter is transformed to the amorphous phase due to the rapid stress release which was consistent with the previous simulations. On the contrary, the main part of β-Sn under spherical indenter remains stable

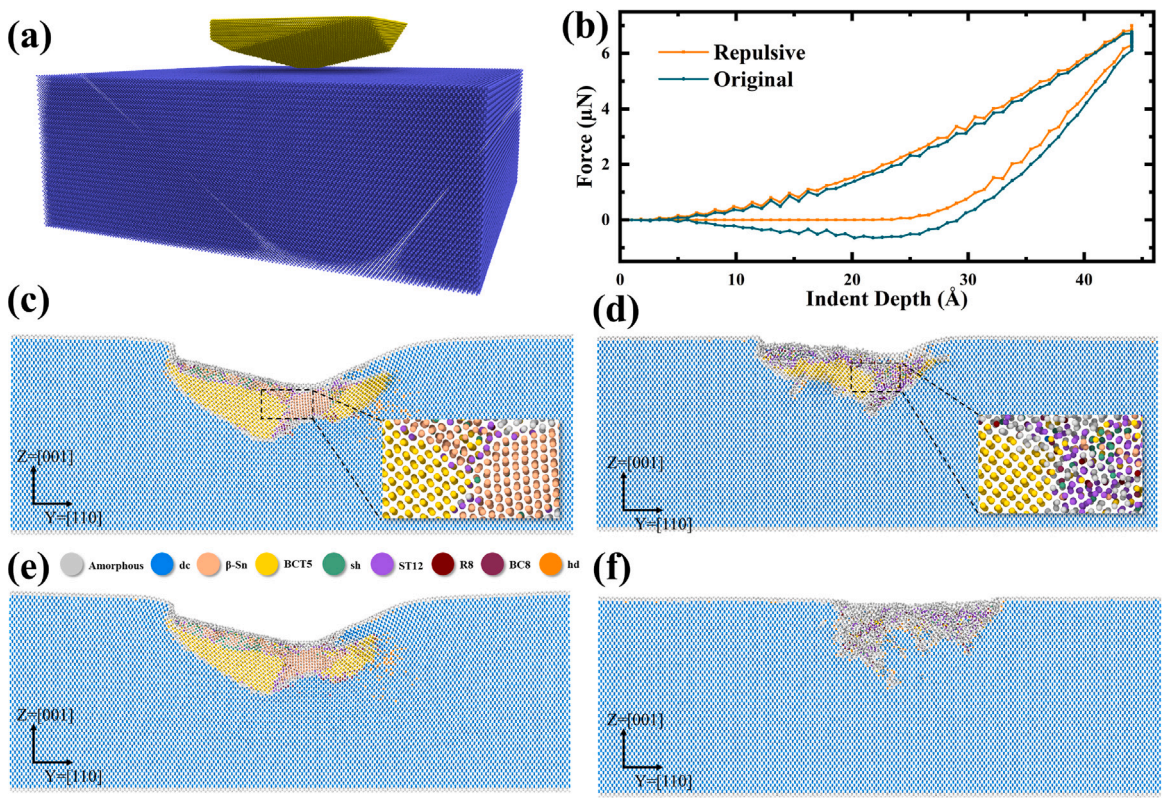

Fig. 2. (a) 3D schematic diagram of the system with Berkovich indenter; (b) force versus indentation depth profiles of the simulation using the original Morse potential and only the repulsive part of the Morse potential. The lateral cross-section views of phase distribution obtained by the original Morse potential at the maximum loading depth of 5 nm (c) and full extraction of the tip (d). Correspondingly, the lateral cross-section views of phase distribution as obtained by the repulsive Morse potential at the maximum loading depth of 5 nm (e) and full extraction of the tip (f). All the phases were recognized by NN-PR method.

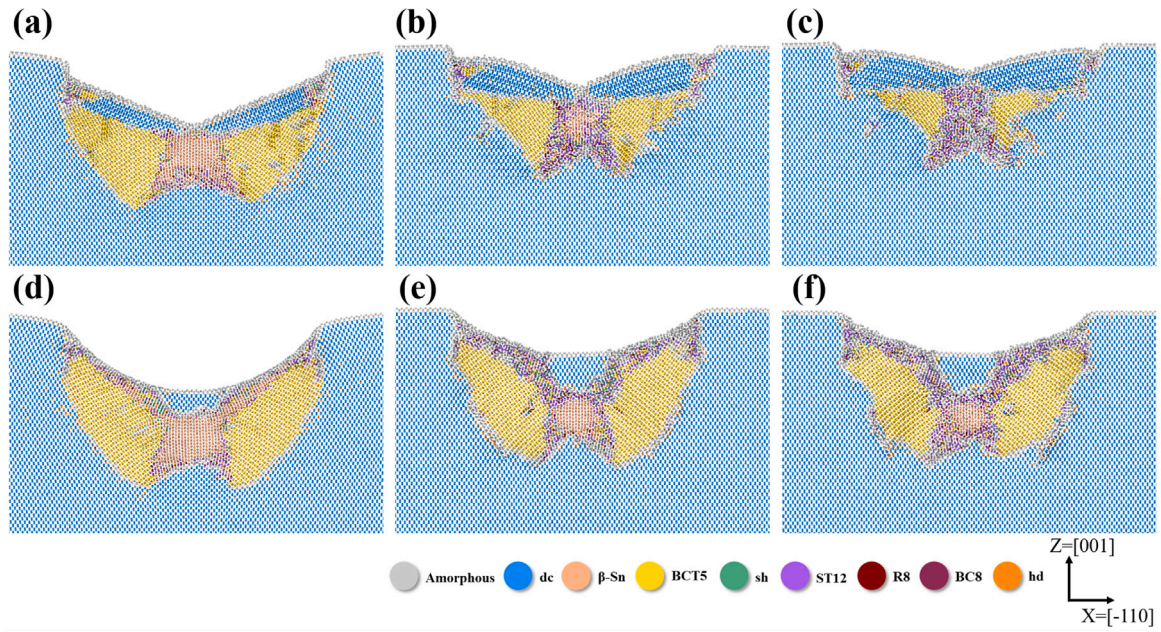

Fig. 3. Side cross-section views of phase distribution obtained from indentation with the Berkovich indenter (a)–(c) and the spherical indenter (d)–(e); (a), (d) Maximum loading depth is 7 nm; (d), (e) Indentation depth of 3 nm during unloading; (c), (f) Full extraction.

upon full extraction of the tip. This transformation was quantified and shown plotted on the profiles of Fig. 4. Here it is shown the evolution of the Phase Fraction (number of atoms in the β-Sn phase divided by the total number of atoms in phases different than dc) during the simulation time. The stability of β-Sn can be strongly correlated with the stress conditions reached in the simulation cell. The β-Sn phase is formed directly beneath the Berkovich indenter. During unloading, with the effect of volume expansion produced by the recovery of BCT5, the β-Sn can be easily transformed into the amorphous structure by releasing the stress along the vertical direction. On the contrary, the

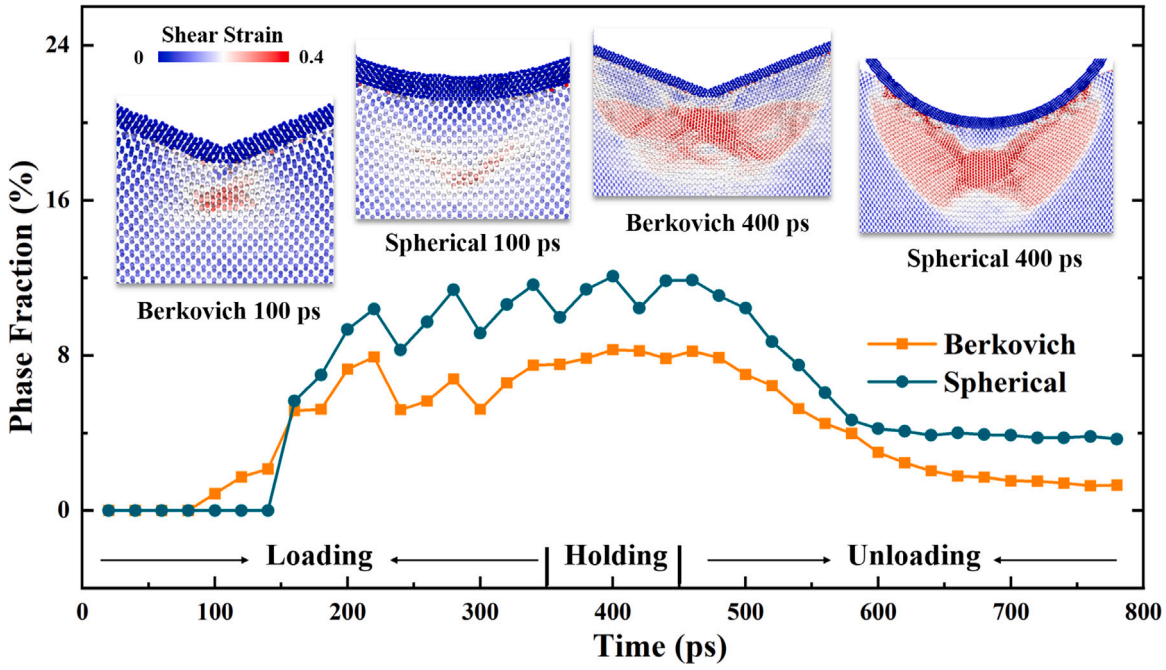

Fig. 4. Evolution of Phase Fraction (number of atoms of β-Sn/number of atom other than dc) during the simulations time. The insets show the side cross-section views at different stages of the indentation process and the atom color specifies the shear strain level. (For interpretation of the references to color in this figure legend, the reader is referred to the web version of this article.)

β-Sn phase formed beneath the spherical indenter is embedded in an upper diamond structure, which plays a role in preventing stress release and maintaining the β-Sn structure stable during the unloading process. The two simulations here discussed for the Berkovich and spherical indenter tips are also included as movie files showing the entire indentation process and named Supplementary Movie 1 and Supplementary Movie 2, respectively.

It is then interesting to investigate the reasons for the different distributions of phases under the different indenter tips. According to the insets in Fig. 4, the maximum shear stress was located at different positions with the different indenter tips before the formation of high-pressure phases. This indicates that the application of shear stress can effectively promote the transformation from diamond cubic to β-Sn, consistent with previously reported results [60,61].

Although the above indentation systems provide precious details on the formation mechanisms of high-pressure Si phases, it is arguable whether the description of the phase transition is accurate and realistic. For instance, the BCT5 structure was never clearly identified in the indentation experiments. This motivated us to explore a more accurate potential, as will be extensively discussed in the next Section.

3.3. *Effect of interatomic potential between silicon atoms*

GAP is a ML interatomic potential based on the Gaussian process regression [37]. The GAP for silicon was originally developed as a general-purpose interatomic potential showing an accurate description of the energy of a wide range of configurations [48]. In Fig. 5 we directly compare formation energies as obtained by Tersoff, GAP and DFT calculations for some of the most relevant Si phases. It can be easily observed that GAP and DFT calculations are in excellent agreement. The general trend of increasing energy with increasing density of the phase is fully captured by GAP, while Tersoff predictions fail to reproduce this behavior. In particular, the high-density BCT5 phase shows formation energy that is lower or comparable to much less dense phases like BC8/R8, thus mistaking the relative phase stability under high-pressure conditions.

Despite its advantages, the application of GAP for MD simulations requires a huge computation effort, particularly compared to semi-empirical potentials like Tersoff. It is almost impossible to carry on the indentation simulation using the same system described in the previous Section, without scaling down its dimensions. We thus prepared a new smaller system by carefully testing the stress convergence on the boundaries. The chosen substrate has the dimensions of $19.63 \times 19.63 \times 9.68$ nm^3 containing 186 576 atoms, while the spherical indenter has a radius of 4 nm, and a maximum loading depth of 3 nm, setting the indenter speed to 1 Å/ps.

The lateral cross-section views of the simulation results obtained by using the Tersoff potential are presented in Fig. 6(a–c) at different stages of the indentation process. It is worth noting that the phase distribution produced with this smaller radius for the spherical indenter tip qualitatively is still consistent with the description reported in the previous Section. Fig. 6(d–f) show the results obtained by the GAP simulation. During the indentation simulation the first phase transition observed is the formation of a small β-Sn nucleus under the indenter, starting at a contact pressure of about 11.6 GPa. This value is in agreement with direct experimental observations of the dc to β-Sn transition, happening between 10 to 12 GPa, as measured in anvil cell experiments [62]. A difference that distinguishes the results obtained by GAP from those of Tersoff is the absence of BCT5 structure. This fact can be attributed to the unfavorable energy of the BCT5 phase compared with other high-pressure phases, according to the formation energy values in Fig. 5. The main phase formed in the deformed volume appears to be a mixture of β-Sn and simple hexagonal (sh). These two phases have very close formation energies predicted by GAP, in agreement with DFT calculations. Moreover, as demonstrated by other *ab initio* studies [63] the cells of these two structures are very similar and are separated by a very low energy barrier (less than 0.01 eV/atom), thus possibly explaining their coexistence under high stresses. We notice that we

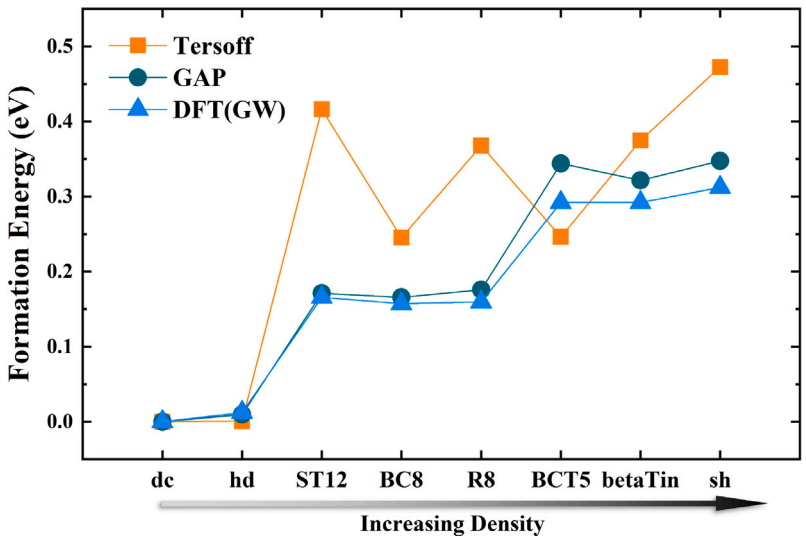

Fig. 5. Formation energy of different silicon phases as calculated by Tersoff and GAP interatomic potentials and DFT calculations. The phases are ordered in term of increasing density.

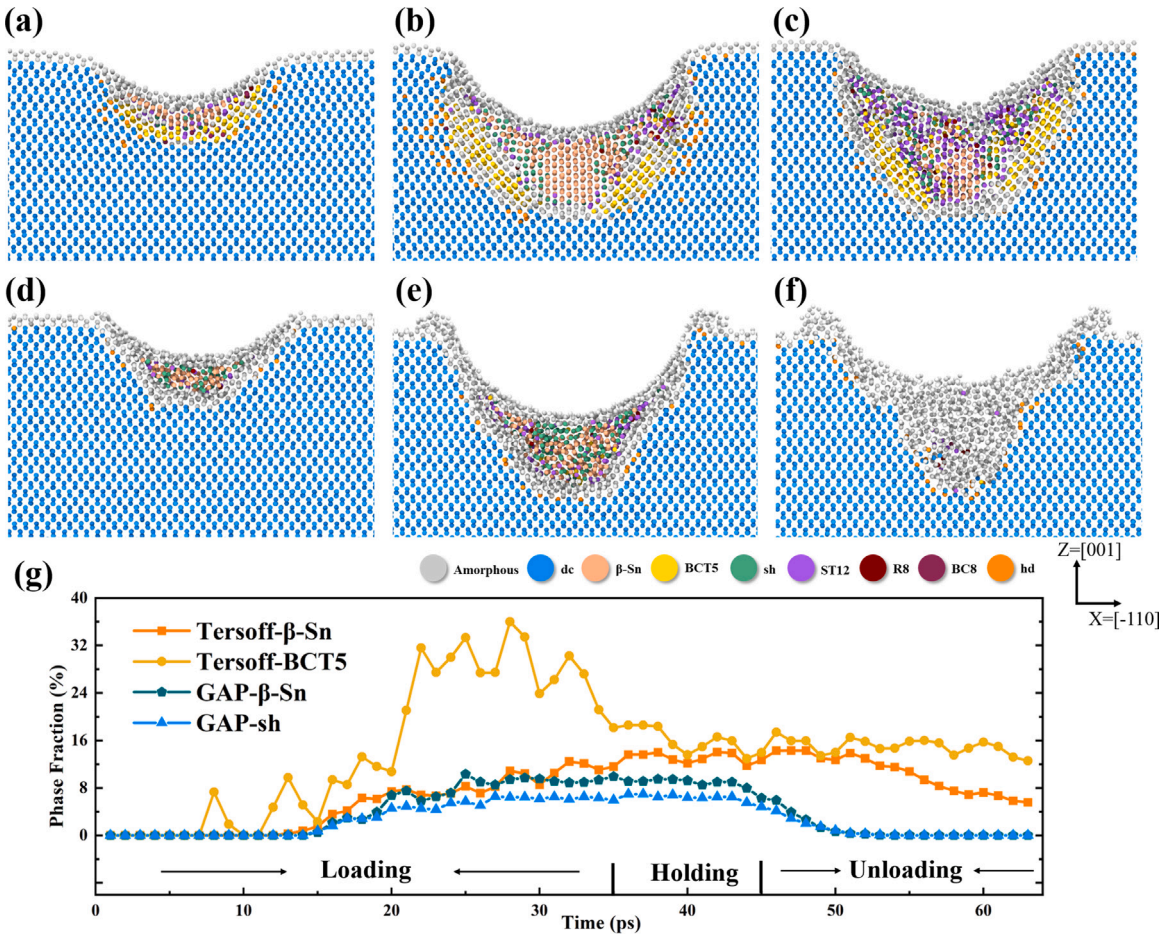

Fig. 6. The side cross-section views of phase distribution with (a–c) Tersoff and (d–e) GAP; (a), (d) Indentation depth = 1.5 nm during loading; (d), (e) Maximum loading depth = 3 nm; (c), (f) Full extraction; (g) Evolution of the Phase Fraction of β-Sn and BCT5 in Tersoff, β-Sn and sh in GAP during the simulation time.

do not observe dislocation nucleation in our indentation simulation. Dislocation injection is an important plastic relaxation mechanism, alternative to phase transition in a nanoindentation experiment. The ability to nucleate and model the subsequent dislocation glide is thus an important feature of a potential used for modeling nanoindentation. As we demonstrate in the Supplementary Material Section S4, under the proper conditions the GAP potential nucleates a dislocation with a critical stress very close to the prediction by the SW potential. The absence of dislocations in the indentation simulation of Fig. 6(d)–(f) should thus be read as a feature of the deformation process under the

present conditions, and not a lack due to the potential not being able to model dislocation nucleation.

At later stages, the metastable phases formed are completely transformed to amorphous after full extraction of the tip. This result appears in agreement with the experimental observation of β-Sn phase transformation into aSi [23,64] in experiments using a high release rate. The evolution of β-Sn and BCT5 phases in Tersoff versus β-Sn and sh phases in GAP are illustrated in Fig. 6(g). Finally, we note that some atom extrusion on the surface can be observed in the simulation using GAP, as also observed in experiments [65]. In general, without claiming perfection, we conclude that the GAP potential provides an unprecedented atomic-scale description of the phase transformation during indentation. The two simulations here discussed, exploiting the Tersoff and GAP interatomic potentials, are also included as movie files showing the entire indentation process and named Supplementary Movie 3 and Supplementary Movie 4, respectively.

Finally, it is worth noticing that recent alternative ML potentials have been demonstrated to be computationally more efficient than GAP [38,39]. In particular, the PACE potential, as discussed in details in Ref. [38], has been demonstrated to be among the best ML potentials developed so far in terms of computational efficiency. Furthermore, the implementation of PACE for silicon has been trained on the same database of the GAP silicon potential. However, based on the detailed comparative simulations reported in the Supplementary Material Section S3, there is considerable doubt as to whether PACE is fully reliable for the specific case of large scale nanoindentation simulations.

4. Conclusions

In this work, we showed that a suitable, synergic use of ML-based approaches allows for noticeable improvements in the simulation of silicon phase transitions during nanoindentation. An advanced NN phase recognition method has been properly developed for Si allotropes and an accurate ML interatomic potential has been exploited for the MD simulations. This allowed us to obtain a realistic description of phase transitions in nanoindentation simulations, providing several important details shedding light on the pressure-induced PTs in Si and clarifying crucial aspects for the atomistic simulations of nanoindentation.

In particular, we first showed how simulations based on Tersoff potential are still useful to evaluate general mechanical aspect of the nanoindentation, like the shape of the indenter and the kind of interaction between the indenter and the substrate (purely repulsive or not). We showed that the phases produced under high-pressure conditions remains stable after fully extracting the indenter only if the interaction between the indenter tip and substrate is properly treated. Furthermore, the effect of the tip geometry has been investigated by directly comparing the spherical and Berkovich tip geometries, linking the observed differences in PTs behavior to the different geometry of the imposed stress field.

Moreover, the stability of the two main phases produced during Tersoff simulations, β-Sn and BCT5, has been critically discussed with the help of DFT calculations for the formation energies of Si allotropes. These results have been directly compared with high-pressure phases obtained by analogous simulations performed with the GAP potential, particularly manifesting: (i) the absence of BCT5 structure; (ii) a complete transition to amorphous during unloading with (iii) atom extrusion on the surface. These phenomena are all consistent with the observations made in nanoindentation experiments.

Declaration of competing interest

The authors declare that they have no known competing financial interests or personal relationships that could have appeared to influence the work reported in this paper.

Acknowledgments

The authors acknowledge the CINECA consortium under the ISCRA initiative for the availability of high-performance computing resources and support.

E.S. acknowledge the Italian Ministry of University and Research for founding the project “SiGe Hexagonal Diamond Phase by nanoindentation”, project number: 2022-NAZ-0098.

Appendix A. Supplementary data

Supplementary material related to this article can be found online at https://doi.org/10.1016/j.actamat.2023.119465.

References

[1] J.J. Gilman, Why silicon is hard, Science 261 (5127) (1993) 1436–1439.
[2] J. Samuels, S.G Roberts, P.B Hirsch, The brittle-to-ductile transition in silicon, Mater. Sci. Eng. A 105–106 (1988) 39–46.
[3] Jodie E. Bradby, James S. Williams, Jennifer Wong-Leung, Michael V. Swain, Paul Munroe, Transmission electron microscopy observation of deformation microstructure under spherical indentation in silicon, Appl. Phys. Lett. 77 (2000) 3749–3751.
[4] J.E. Bradby, J.S. Williams, J. Wong-Leung, M.V. Swain, P. Munroe, Mechanical deformation in silicon by micro-indentation, J. Mater. Res. 16 (5) (2001) 1500–1507.
[5] M.S.R.N. Kiran, T.T. Tran, L.A. Smillie, B. Haberl, D. Subianto, J.S. Williams, J.E. Bradby, Temperature-dependent mechanical deformation of silicon at the nanoscale: Phase transformation versus defect propagation, J. Appl. Phys. 117 (20) (2015) 205901.
[6] Kausala Mylvaganam, L.C. Zhang, Nanotwinning in monocrystalline silicon upon nanoscratching, Scr. Mater. 65 (3) (2011) 214–216.
[7] Brad D. Malone, Jay D. Sau, Marvin L. Cohen, Ab initio study of the optical properties of Si-XII, Phys. Rev. B 78 (2008) 161202.
[8] S. Wong, B. Haberl, B.C. Johnson, A. Mujica, M. Guthrie, J.C. McCallum, J.S. Williams, J.E. Bradby, Formation of an r8-dominant Si material, Phys. Rev. Lett. 122 (2019) 105701.
[9] Haidong Zhang, Hanyu Liu, Kaya Wei, Oleksandr O. Kurakevych, Yann Le Godec, Zhenxian Liu, Joshua Martin, Michael Guerrette, George S. Nolas, Timothy A. Strobel, BC8 silicon (Si-III) is a narrow-gap semiconductor, Phys. Rev. Lett. 118 (2017) 146601.
[10] Håkon Ikaros T. Hauge, Marcel A. Verheijen, Sonia Conesa-Boj, Tanja Etzelstorfer, Marc Watzinger, Dominik Kriegner, Ilaria Zardo, Claudia Fasolato, Francesco Capitani, Paolo Postorino, Sebastian Kölling, Ang Li, Simone Assali, Julian Stangl, Erik P.A.M. Bakkers, Hexagonal silicon realized, Nano Lett. 15 (9) (2015) 5855–5860.
[11] Sven Barth, Michael S. Seifner, Stephen Maldonado, Metastable group IV allotropes and solid solutions: Nanoparticles and nanowires, Chem. Mater. 32 (7) (2020) 2703–2741.
[12] Brad D. Malone, Jay D. Sau, Marvin L. Cohen, Ab initio survey of the electronic structure of tetrahedrally bonded phases of silicon, Phys. Rev. B 78 (2008) 035210.
[13] A. Mujica, Angel Rubio, A. Muñoz, R.J. Needs, High-pressure phases of group-IV, III-V, and II-VI compounds, Rev. Modern Phys. 75 (3) (2003) 863–912.
[14] Cong Li, Jiajia Wang, Lihui Yan, Bin Deng, Xingjun Liu, A comprehensive study of the high-pressure–temperature phase diagram of silicon, J. Mater. Sci. 53 (2018).
[15] Silvia Pandolfi, S. Brennan Brown, P.G. Stubley, Andrew Higginbotham, C.A. Bolme, H.J. Lee, B. Nagler, E. Galtier, R.L. Sandberg, W. Yang, W.L. Mao, J.S. Wark, A.E. Gleason, Atomistic deformation mechanism of silicon under laser-driven shock compression, Nature Commun. 13 (1) (2022) 5535.
[16] A. Kailer, Y.G. Gogotsi, K.G. Nickel, Phase transformations of silicon caused by contact loading, J. Appl. Phys. 81 (7) (1997) 3057–3063.
[17] Jae-il Jang, M.J. Lance, Songqing Wen, Ting Y. Tsui, G.M. Pharr, Indentation-induced phase transformations in silicon: influences of load, rate and indenter angle on the transformation behavior, Acta Mater. 53 (6) (2005) 1759–1770.
[18] Mangalampalli S.R.N. Kiran, Bianca Haberl, Jodie E. Bradby, James S. Williams, Chapter five - nanoindentation of silicon and germanium, in: Lucia Romano, Vittorio Privitera, Chennupati Jagadish (Eds.), Defects in Semiconductors, in: Semiconductors and Semimetals, vol. 91, Elsevier, 2015, pp. 165–203.
[19] Yvonne B. Gerbig, Chris A. Michaels, Robert F. Cook, In situ observation of the spatial distribution of crystalline phases during pressure-induced transformations of indented silicon thin films, J. Mater. Res. 30 (3) (2015) 390–406.
[20] V. Domnich, Y. Gogotsi, Phase transformations in silicon under contact loading, Rev. Adv. Mater. Sci. 3 (2002) 1–36.

[21] Tao Liang, Lianghua Xiong, Hongbo Lou, Fujun Lan, Junran Zhang, Ye Liu, Dongsheng Li, Qiaoshi Zeng, Zhidan Zeng, Mechanical properties of hexagonal silicon, Scr. Mater. 220 (2022) 114936.

[22] Silvia Pandolfi, Carlos Renero-Lecuna, Yann Le Godec, Benoit Baptiste, Nicolas Menguy, Michele Lazzeri, Christel Gervais, Kristina Spektor, Wilson A. Crichton, Oleksandr O. Kurakevych, Nature of hexagonal silicon forming via high-pressure synthesis: Nanostructured hexagonal 4H polytype, Nano Lett. 18 (9) (2018) 5989–5995.

[23] Chuanlong Lin, Xuqiang Liu, Dongliang Yang, Xiaodong Li, Jesse S. Smith, Bihan Wang, Haini Dong, Shourui Li, Wenge Yang, John S. Tse, Temperature- a nd rate-dependent pathways in formation of metastable silicon phases under rapid decompression, Phys. Rev. Lett. 125 (15) (2020).

[24] Hyung-Jun Chang, Marc Fivel, David Rodney, Marc Verdier, Multiscale modelling of indentation in FCC metals: From atomic to continuum, C. R. Phys. 11 (3–4) (2010) 285–292.

[25] K. Mulewska, F. Rovaris, F.J. Dominguez-Gutierrez, W.Y. Huo, D. Kalita, I. Jozwik, S. Papanikolaou, M.J. Alava, L. Kurpaska, J. Jagielski, Self-ion irradiation effects on nanoindentation-induced plasticity of crystalline iron: A joint experimental and computational study, Nucl. Instrum. Methods Phys. Res. B 539 (2023) 55–61.

[26] Rafał Abram, Dariusz Chrobak, Jesper Byggmästar, Kai H Nordlund, Roman Nowak, Silicon nanoindentation modelled by hybrid potential, 2022, arXiv preprint arXiv:2207.08102.

[27] J.J. Tersoff, Modeling solid-state chemistry: Interatomic potentials for multicomponent systems, Phys. Rev. B 39 (8) (1989) 5566.

[28] J. Tersoff, Erratum: Modeling solid-state chemistry: Interatomic potentials for multicomponent systems, Phys. Rev. B 41 (1990) 3248.

[29] Saurav Goel, Nadimul Haque Faisal, Xichun Luo, Jiwang Yan, Anupam Agrawal, Nanoindentation of polysilicon and single crystal silicon: Molecular dynamics simulation and experimental validation, J. Phys. D: Appl. Phys. 47 (27) (2014) 275304.

[30] D.E. Kim, S.I. Oh, Atomistic simulation of structural phase transformations in monocrystalline silicon induced by nanoindentation, Nanotechnology 17 (9) (2006) 2259.

[31] Sanshan Jiao, Qiming Huang, Wenjing Tu, Jian Chen, Zhengming Sun, Investigation on the phase transformation of monocrystalline silicon during nanoindentation at cryogenic temperature by molecular dynamics simulation, Physica B 555 (2019) 139–144.

[32] Lin Zhang, Jiwang Yan, Evolution of high-pressure metastable phase Si-XIII during silicon nanoindentation: A molecular dynamics study, Comput. Mater. Sci. 191 (2021) 110344.

[33] Y.B. Gerbig, C.A. Michaels, A.M. Forster, R.F. Cook, In situ observation of the indentation-induced phase transformation of silicon thin films, Phys. Rev. B 85 (2012) 104102.

[34] Yvonne B. Gerbig, Chris A. Michaels, Robert F. Cook, In situ observations of Berkovich indentation induced phase transitions in crystalline silicon films, Scr. Mater. 120 (2016) 19–22.

[35] Rafal Abram, Dariusz Chrobak, Jesper Byggmästar, Kai Nordlund, Roman Nowak, Comprehensive structural changes in nanoscale-deformed silicon modelled with an integrated atomic potential, Materialia 28 (2023) 101761.

[36] Lars Pastewka, Andreas Klemenz, Peter Gumbsch, Michael Moseler, Screened empirical bond-order potentials for Si-C, Phys. Rev. B 87 (2013) 205410.

[37] Albert P Bartók, Mike C Payne, Risi Kondor, Gábor Csányi, Gaussian approximation potentials: The accuracy of quantum mechanics, without the electrons, Phys. Rev. Lett. 104 (13) (2010) 136403.

[38] Yury Lysogorskiy, Cas van der Oord, Anton Bochkarev, Sarath Menon, Matteo Rinaldi, Thomas Hammerschmidt, Matous Mrovec, Aidan Thompson, Gábor Csányi, Christoph Ortner, Ralf Drautz, Performant implementation of the atomic cluster expansion (PACE) and application to copper and silicon, NPJ Comput. Mater. 7 (1) (2021) 97.

[39] Yunxing Zuo, Chi Chen, Xiangguo Li, Zhi Deng, Yiming Chen, Jörg Behler, Gábor Csányi, Alexander V. Shapeev, Aidan P. Thompson, Mitchell A. Wood, Shyue Ping Ong, Performance and cost assessment of machine learning interatomic potentials, J. Phys. Chem. A 124 (4) (2020) 731–745.

[40] Jörg Behler, Michele Parrinello, Generalized neural-network representation of high-dimensional potential-energy surfaces, Phys. Rev. Lett. 98 (2007) 146401.

[41] G.J. Ackland, A.P. Jones, Applications of local crystal structure measures in experiment and simulation, Phys. Rev. B 73 (5) (2006) 054104.

[42] Alexander Stukowski, Structure identification methods for atomistic simulations of crystalline materials, Modelling Simul. Mater. Sci. Eng. 20 (4) (2012) 045021.

[43] Emanuel A. Lazar, Jian Han, David J. Srolovitz, Topological framework for local structure analysis in condensed matter, Proc. Natl. Acad. Sci. 112 (43) (2015) E5769–E5776.

[44] Peter Mahler Larsen, Søren Schmidt, Jakob Schiøtz, Robust structural identification via polyhedral template matching, Modelling Simul. Mater. Sci. Eng. 24 (5) (2016) 055007.

[45] Peter M. Larsen, Revisiting the common neighbour analysis and the centrosymmetry parameter, 2020, arXiv:2003.08879.

[46] Heejung W. Chung, Rodrigo Freitas, Gowoon Cheon, Evan J. Reed, Data-centric framework for crystal structure identification in atomistic simulations using machine learning, Phys. Rev. Mater. 6 (4) (2022).

[47] W.C.D. Cheong, L.C. Zhang, Molecular dynamics simulation of phase transformations in silicon monocrystals due to nano-indentation, Nanotechnology 11 (3) (2000) 173.

[48] Albert P Bartók, James Kermode, Noam Bernstein, Gábor Csányi, Machine learning a general-purpose interatomic potential for silicon, Phys. Rev. X 8 (4) (2018) 041048.

[49] Steve Plimpton, Fast parallel algorithms for short-range molecular dynamics, J. Comput. Phys. 117 (1) (1995) 1–19.

[50] Alexander Stukowski, Visualization and analysis of atomistic simulation data with OVITO–the open visualization tool, Modelling Simul. Mater. Sci. Eng. 18 (1) (2009) 015012.

[51] John P. Perdew, Kieron Burke, Matthias Ernzerhof, Generalized gradient approximation made simple, Phys. Rev. Lett. 77 (1996) 3865–3868.

[52] G. Kresse, J. Furthmüller, Efficient iterative schemes for ab initio total-energy calculations using a plane-wave basis set, Phys. Rev. B 54 (1996) 11169–11186.

[53] P.E. Blöchl, Projector augmented-wave method, Phys. Rev. B 50 (1994) 17953–17979.

[54] Ian Goodfellow, Yoshua Bengio, Aaron Courville, Deep Learning, MIT Press, 2016.

[55] Albert P. Bartók, Risi Kondor, Gábor Csányi, On representing chemical environments, Phys. Rev. B 87 (18) (2013) 184115.

[56] Lauri Himanen, Marc O.J. Jäger, Eiaki V. Morooka, Filippo Federici Canova, Yashasvi S. Ranawat, David Z. Gao, Patrick Rinke, Adam S. Foster, Dscribe: Library of descriptors for machine learning in materials science, Comput. Phys. Comm. 247 (2020) 106949.

[57] Anubhav Jain, Shyue Ping Ong, Geoffroy Hautier, Wei Chen, William Davidson Richards, Stephen Dacek, Shreyas Cholia, Dan Gunter, David Skinner, Gerbrand Ceder, Kristin A. Persson, Commentary: The materials project: A materials genome approach to accelerating materials innovation, APL Mater. 1 (1) (2013) 011002.

[58] Van-Trung Pham, Te-Hua Fang, Interfacial mechanics and shear deformation of indented germanium on silicon (001) using molecular dynamics, Vacuum 173 (2020) 109184.

[59] Xiancheng Du, Hongwei Zhao, Lin Zhang, Yihan Yang, Hailong Xu, Haishuang Fu, Lijia Li, Molecular dynamics investigations of mechanical behaviours in monocrystalline silicon due to nanoindentation at cryogenic temperatures and room temperature, Sci. Rep. 5 (1) (2015) 16275.

[60] Katalin Gaál-Nagy, Dieter Strauch, Transition pressures and enthalpy barriers for the cubic diamond $\rightarrow$ β-tin transition in Si and Ge under nonhydrostatic conditions, Phys. Rev. B 73 (13) (2006) 134101.

[61] Dong Earn Kim, Soo Ik Oh, Deformation pathway to high-pressure phases of silicon during nanoindentation, J. Appl. Phys. 104 (1) (2008) 013502.

[62] Cong Li, Cuiping Wang, Jiajia Han, Lihui Yan, Bin Deng, Xingjun Liu, A comprehensive study of the high-pressure–temperature phase diagram of silicon, J. Mater. Sci. 53 (10) (2018) 7475–7485.

[63] Richard J. Needs, Richard M. Martin, Transition from β-tin to simple hexagonal silicon under pressure, Phys. Rev. B 30 (1984) 5390–5392.

[64] Tom Juliano, Yury Gogotsi, Vladislav Domnich, Effect of indentation unloading conditions on phase transformation induced events in silicon, J. Mater. Res. 18 (5) (2003) 1192–1201.

[65] Sun Jiapeng, Li Cheng, Jing Han, Aibin Ma, Liang Fang, Nanoindentation induced deformation and pop-in events in a silicon crystal: molecular dynamics simulation and experiment, Sci. Rep. 7 (1) (2017) 10282.